N O T I C E

THIS DOCUMENT HAS BEEN REPRODUCED FROM MICROFICHE. ALTHOUGH IT IS RECOGNIZED THAT CERTAIN PORTIONS ARE ILLEGIBLE, IT IS BEING RELEASED IN THE INTEREST OF MAKING AVAILABLE AS MUCH INFORMATION AS POSSIBLE

JPL NO. 9950-553

DOE/JPL-955640-81/5
DISTRIBUTION CATEGORY UC-63

DEVELOPMENT AND FABRICATION OF A SOLAR CELL JUNCTION PROCESSING SYSTEM

QUARTERLY PROGRESS REPORT NO.5
APRIL 1981

THE JPL LOW-COST SOLAR ARRAY PROJECT IS SPONSORED BY THE U.S. DEPARTMENT OF ENERGY AND FORMS PART OF THE SOLAR PHOTOVOLTAIC CONVERSION PROGRAM TO INITIATE A MAJOR EFFORT TOWARD THE DEVELOPMENT OF LOW-COST SOLAR ARRAYS. THIS WORK WAS PERFORMED FOR THE JET PROPULSION LABORATORY, CALIFORNIA INSTITUTE OF TECHNOLOGY BY AGREEMENT BETWEEN NASA AND DOE.

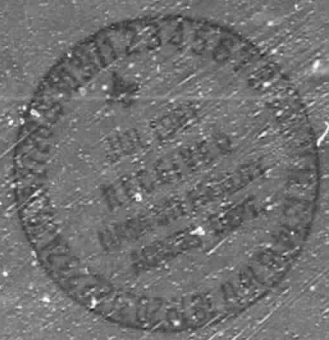

PREPARED UNDER CONTRACT NO. 955640 FOR
JET PROPULSION LABORATORY
CALIFORNIA INSTITUTE OF TECHNOLOGY
PASADENA, CALIFORNIA 91103

(NASA-CR-164444) DEVELOPMENT AND FABRICATION OF A SOLAR CELL JUNCTION PROCESSING SYSTEM Quarterly Progress Report, 1 Jan. 31 Mar. 1980 (Spire Corp., Bedford, Mass.) 33 p HC A03/MF A01 CSCL 10A G3/44

N81-25497

Unclas
26608

Spire

"This report was prepared as an account of work sponsored by the United States Government. Neither the United States nor the United States Department of Energy, nor any of their employees, nor any of their contractors, subcontractors, or their employees, makes any warranty, express or implied, or assumes any legal liability or responsibility for the accuracy, completeness or usefulness of any information, apparatus, product or process disclosed, or represents that its use would not infringe privately owned rights."

DRD No. QR
CDRL Item No. 5

DOE/JPL-955640-81/5
Distribution Category UC-63

DEVELOPMENT AND FABRICATION OF A SOLAR CELL JUNCTION PROCESSING SYSTEM

Report Number QR-10073-05
Quarterly Report

April 1981

This work was performed for the Jet Propulsion Laboratory, California Institute of Technology sponsored by the National Aeronautics and Space Administration under Contract NAS7-100.

Prepared by: _____
Project Engineer

Approved by: _____
Program Manager

SPIRE CORPORATION
Patriots Park
Bedford, MA 01730

TABLE OF CONTENTS

Section		Page
1	CONTRACT OBJECTIVES	1
2	SUMMARY OF WORK PERFORMED	4
	2.1 Introduction	4
	2.2 Pulser Fabrication and Testing	4
	2.3 Task 2. Transport Design	4
3	PROGRESS ON TASK 1 - DEVELOPMENT OF PULSED ELECTRON BEAM SUBSYSTEM	7
	3.1 Fabrication and Testing	7
	3.1.1 Subsystem Description	7
	3.1.2 Pulse Generator	11
	3.1.3 Diode Tests	13
	3.1.4 Annealing Experiments	19
	3.1.5 Material Development	20
4	PLANS	21
5	SCHEDULE	23
6	PROGRESS ON TASK 2 - WAFER TRANSPORT SYSTEM DEVELOPMENT	25
	6.1 Transport Design and Fabrication	25
7	PLANS	26
8	SCHEDULE	27
	REFERENCES	R-1

LIST OF FIGURES

Figure		Page
1	Spire/JPL Junction Processor	2
2	SPI-PULSE 7000 Pulser	5
3	Nested Set of SPI-PULSE 7000 Energy Storage Liners	6
4	Data Comparison of Magnetic Field Versus Current for SPI-PULSE 7000 Collimating Magnet	8
5	Calibration Curve for Diode Voltage Monitor at 100 mV/div and Input Voltage at 7.0 V/div	10
6	(a) Current Signal From Pulse Generator With Diode Shorted Out; 50 kV Charge, 34.5 kA/div, 50 ns/div.	12
	(b) Equivalent Circuit Model for Pulse Generator With Measured Parameters From (a)	12
7	Typical Corrected Diode Voltage, Current and Electron Energy Spectra From Computer Code EBSPEC	16
8	Measured and Modeled Diode Perveance for Pulse Shown in Figure 7	17
9	Perveance at Maximum Power Versus R^2/D^2 for SPI-PULSE 7000 Initial Tests	18
10	SPI-PULSE 700C Assembly and Test Schedule	22
11	Task 1 Schedule	24
12	Task 2 Schedule	28

SECTION 1
CONTRACT OBJECTIVES

The basic objectives of the program are the following:

1. To design, develop, construct and deliver a junction processing system which will be capable of producing solar cell junctions by means of ion implantation followed by pulsed electron beam annealing.
2. To include in the system a wafer transport mechanism capable of transferring 4-inch-diameter wafers into and out of the vacuum chamber where the ion implantation and pulsed electron beam annealing processes take place.
3. To integrate, test and demonstrate the system prior to its delivery to JPL along with detailed operating and maintenance manuals.
4. To estimate component lifetimes and costs, as necessary for the contract, for the performance of comprehensive analyses in accordance with the Solar Array Manufacturing Industry Costing Standards (SAMICS).

In achieving these objectives, Spire will perform five tasks:

Task 1 - Pulsed Electron Beam Subsystem Development

Task 2 - Wafer Transport System Development

Task 3 - Ion Implanter Development

Task 4 - Junction Processing System Integration

Task 5 - Junction Processing System Cost Analyses

Under this contract the automated junction formation equipment to be developed involves a new system design incorporating a modified, government-owned, JPL-controlled ion implanter into a Spire-developed pulsed electron beam annealer and wafer transport system. Figure 1 presents a conceptual drawing of the junction processing system. When modified, the ion implanter will deliver a 16 mA beam of $^{31}P^{+}$ ions with a fluence of 2.5×10^{15} ions per square centimeter at an energy of 10 keV. The throughput design goal rate for the junction processor is 10^{7} four-inch-diameter wafers per year.

ORIGINAL PAGE IS
OF POOR QUALITY

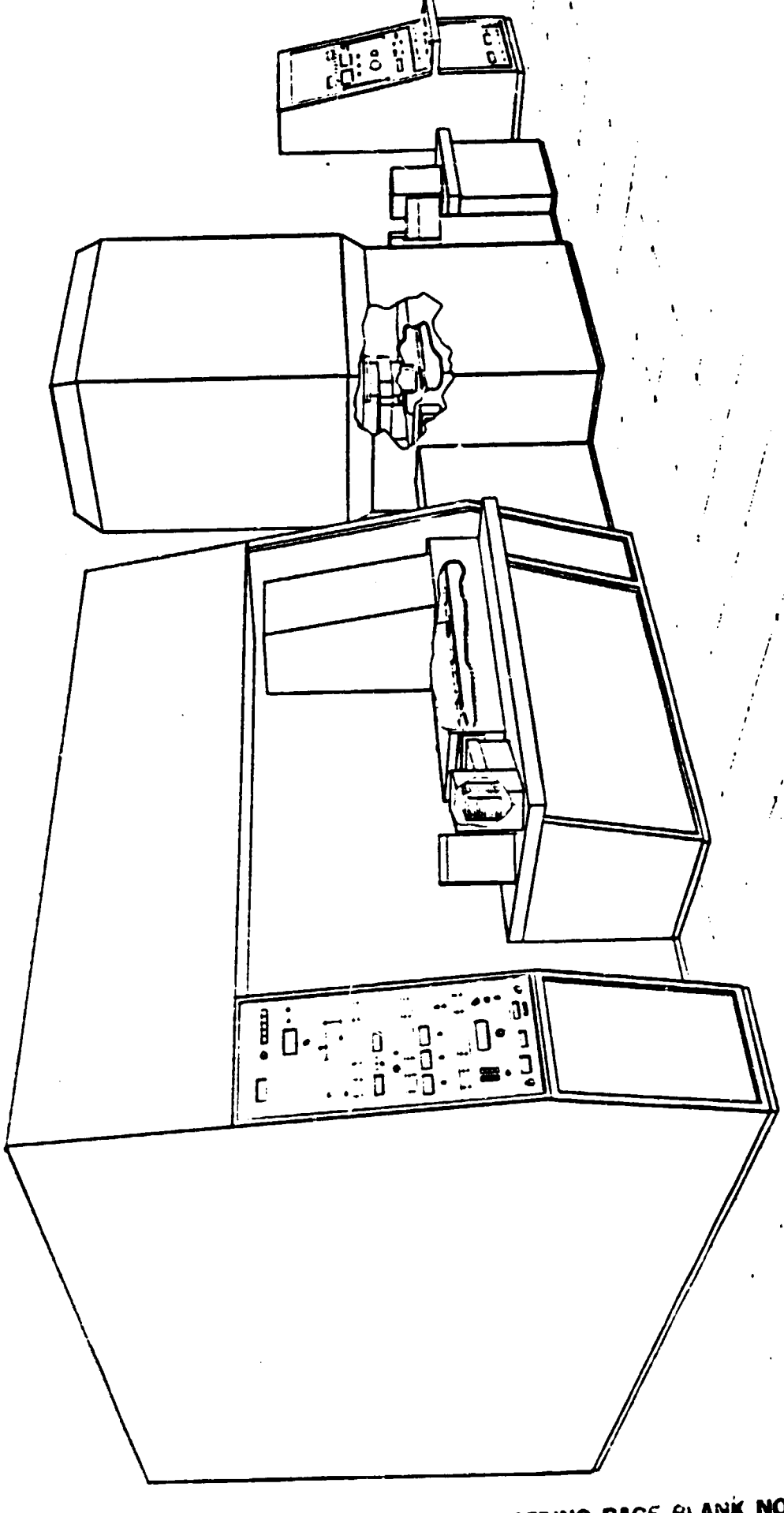

FIGURE 1. SPIRE/JPL JUNCTION PROCESSOR

PRECEDING PAGE BLANK NOT FILMED

At the present time, authorization has been given to perform work only on Tasks 1 and 2. The performance of Tasks 3, 4 and 5 has been deferred until a written "Notice to Proceed" with one or more of these deferred tasks is received from JPL.

SECTION 2
SUMMARY OF WORK PERFORMED

2.1 INTRODUCTION

This quarterly report covers the work performed during the period 1 January through 31 March 1980 on Tasks 1 and 2 of a contract for the development and fabrication of a solar cell junction processing system. The major component fabrication program has been completed for Task 1. Assembly and system testing has been underway in the development of the pulsed electron beam annealing machine shown in Figure 2. The design program for the Task 2 transport has reached completion, and the detailed drawings have been released for fabrication and procurement of the long lead-time components.

2.2 PULSER FABRICATION AND TESTING

Fabrication of the first stage of the pulsed electron beam annealer was completed. The objective of these initial checks was to test the functioning of its separate subsystems. Appropriate modifications based upon measurements taken are planned for the next quarter. Annealing of four inch wafers at the required rate must await completion of the Task 2 wafer transport development and fabrication.

There were four groups of tests, those of the mechanical and electrical subsystems, pulse generator, electron beam diode and the annealing process. Annealing experiments were begun at the end of March and will continue after modification of the pulser to insure reproducibility and uniformity. Electrical characterization of diode behavior as a function of varying parameters is far advanced. Initial tests of subsystems and the pulse generator are complete using the 160 kV test power supply and the first production run of dielectric liners shown in Figure 3.

2.3 TASK 2. TRANSPORT DESIGN

The complete engineering system design has been formulated, and the accompanying manufacturing detail drawings are about 60 percent complete. The entrance and exit "Y" tracks of the processing chamber have been designed to interconnect with the 50 carrier cassette elevator locks by means of short three-phase transition track sections located between the outside vacuum locks and the processing chamber.

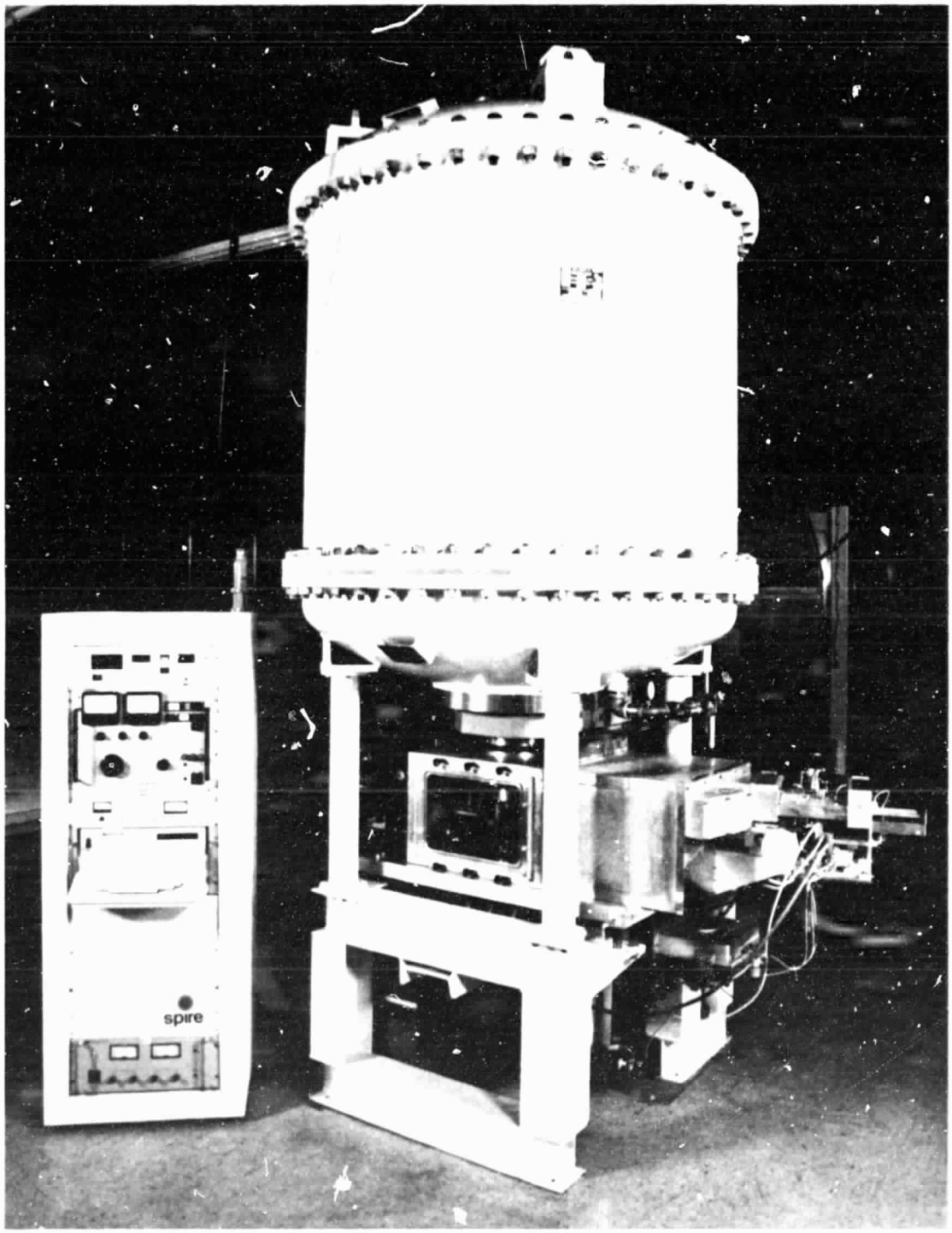

FIGURE 2. SPI-PULSE 7000 PULSER

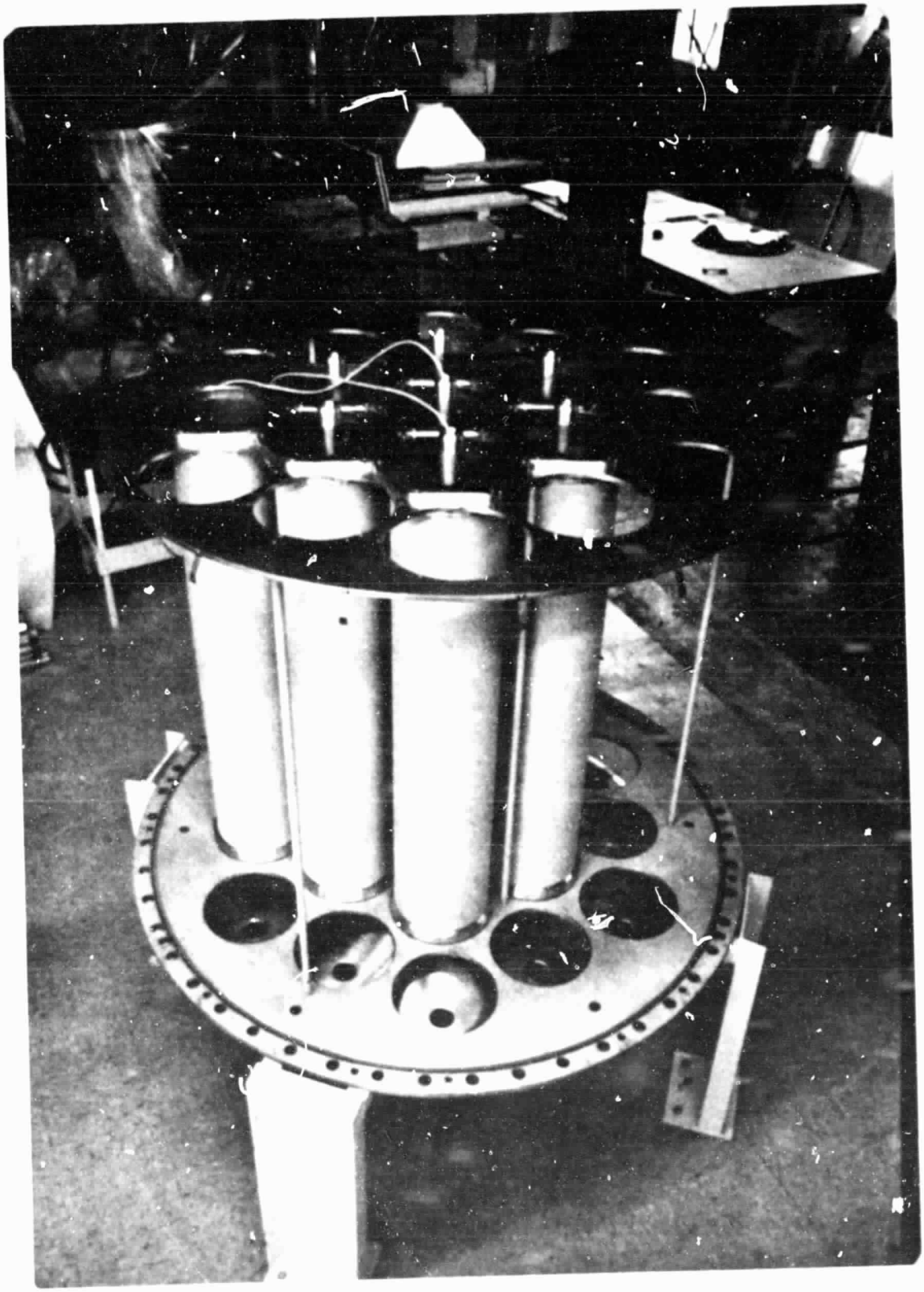

FIGURE 3. NESTED SET OF SPI-PULSE 7000 ENERGY STORAGE LINERS

ORIGINAL PAGE I
OF POOR QUALITY

SECTION 3
PROGRESS ON TASK 1 - DEVELOPMENT OF PULSED ELECTRON BEAM SUBSYSTEM

3.1 PULSER FABRICATION AND TESTING

3.1.1 Subsystem Description

The pulsed electron beam annealer comprises seven separate subsystems. These are the vacuum system, wafer transport, insulating gas supply for the high voltage tank, magnet and its power supply, high voltage power supply, diagnostic equipment and electronic controls.

The microprocessor control system was used for all tests. It was not adversely affected by triggering of the pulse generator. Complete sequential operation of the wafer transport and pulse annealing will be tested under automated control in the next quarter.

The vacuum system for this part of the junction processor was previously tested. It was not affected by pulsed operations. Pressure was maintained below 10^{-6} torr.

The interim wafer transport system was previously tested. In this quarter, the mechanism to lift wafers into place for pulse annealing was added. The system functions satisfactorily at one sample every 3 seconds. There were no adverse effects from the magnetic field at 2 kG or operation of the pulser.

The pulse generator was designed to be insulated by gas at 100 psi. Pure nitrogen was tested and found lacking. A mixture of nitrogen and carbon dioxide functioned satisfactorily at 180 kV charge. Minor changes will be made in the gas pressurization system in the next quarter.

The magnet was tested for power consumption, cooling and field. This system is required for uniform irradiation of the samples. Figure 4 shows the strength of the field as a function of the applied current. The maximum field is limited by saturation effects, particularly evident above 2.5 kG. However, experiments have shown that the optimal field is below 2 kG. At this 2 kG level the magnet draws only 130 watts, significantly below the 3 kW first estimated for this subystem in the original SAMICS analysis. This is a significant savings in total power and cooling requirements.

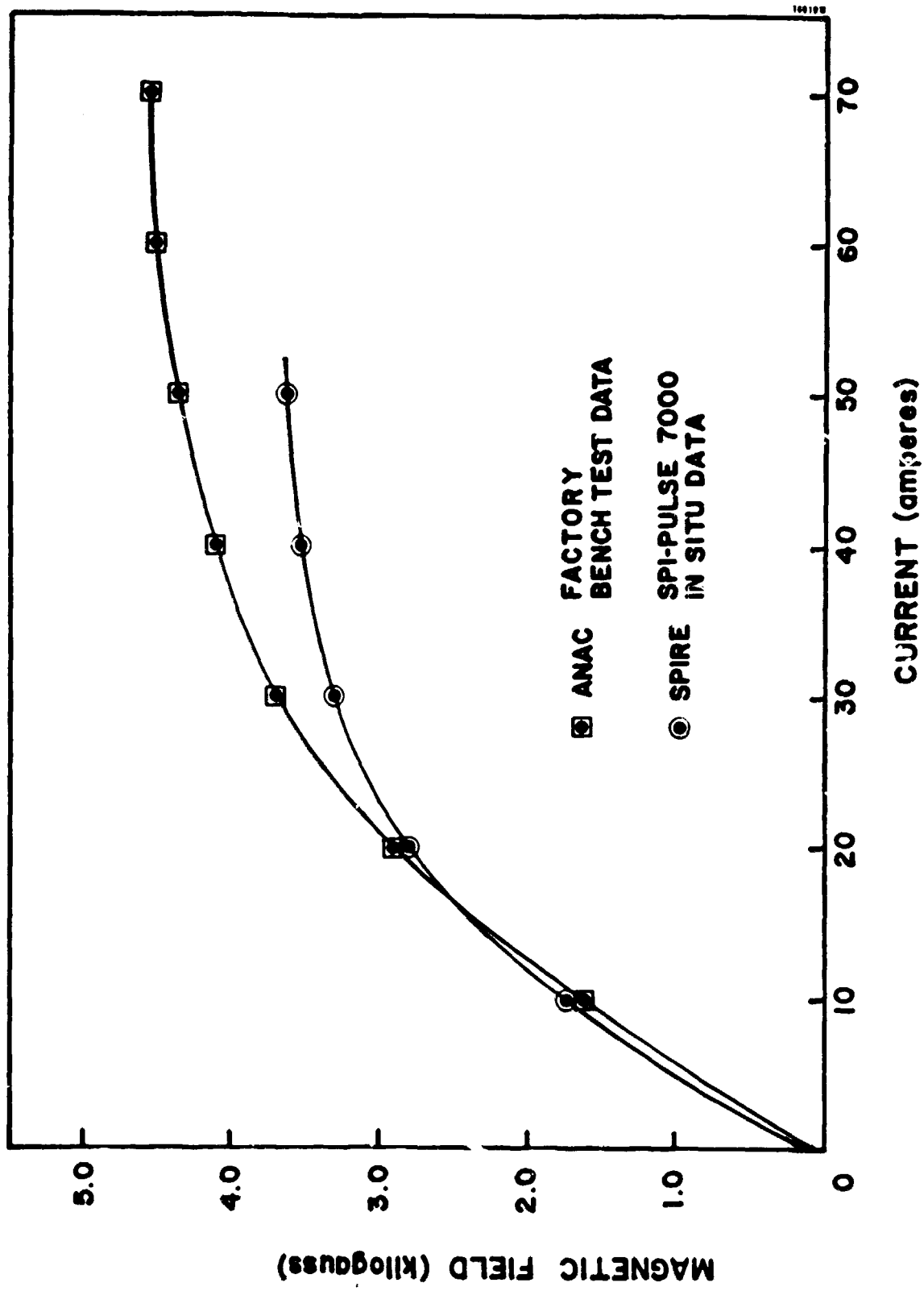

FIGURE 4. DATA COMPARISON OF MAGNETIC FIELD VERSUS CURRENT FOR SPI-PULSE 7000 COLLIMATING MAGNET

The high voltage power supply was inspected and tested. Under load it can deliver 5mA at 160 kV. At no load (minimal current) it can charge the energy store to 180 kV. The higher voltage is restricted to testing only, since the safety interlocks trip after triggering the pulse generator at 180 kV. Modifications to this subsystem are planned for the next quarter.

The diagnostic equipment includes the diode voltage and current monitors, and the electron beam calorimeter. Eventually, the noninterferring diode monitors will provide ths signals to verify operational status of the pulse annealer. For these initial tests, the signals were displayed on oscilloscopes and recorded on film. The diode voltage monitor was calibrated in a circuit using the cathode support shank as the open termination of a 50 ohm coaxial cable, which was energized by a SPI-PULSE^{TM} 25. The pulser signal was split by a calibrated matched tee with one (attenuated) signal displayed on an oscilloscope as the input, and the other line going to the monitor whose output was displayed simultaneously (see Figure 5). From this data the monitor calibration factor was 1710 volts per signal volt output, accurate to 2 percent and traceable to NBS standards. Measured maximum expected error due to cathode support misalignment was less than 3 percent. Measured RC decay time constant was 1.15 microseconds, a correction applied when the signal was analyzed by a computer. The diode current monitor output signal was 73.7 amperes per volt with an uncertainty less than one percent based upon the average of 200 resistors, each 5 percent accurate. The large signals (10V) generated by these monitors were choosen to avoid the need for very high bandwidth amplifiers in later circuitry.

The calorimeter array built for testing the uniformity of the electron beam did not operate properly. Inadequate grounding allowed direct current from the pulse generator discharge to swamp the electronics for reading the signals from the 29 probes. The problem will be corrected in the next quarter. Five of the probes were monitored by an oscilloscope on sequential test shots. The exponential decay time constant for the thermal signal was over 8 seconds for all of the probes tested, implying that the proposed readout every 0.5 second is sufficient. Excluding the short burst of RF noise, the 0.1 mV signals were clean and not affected by 60 Hz ground loop noise. After pulsing the calorimeter for these test shots, the pattern of calorimeter probes became imaged on the cathode. The possibility of ATJ graphite from the calorimeter plate being blown off by the pulse will be investigated.

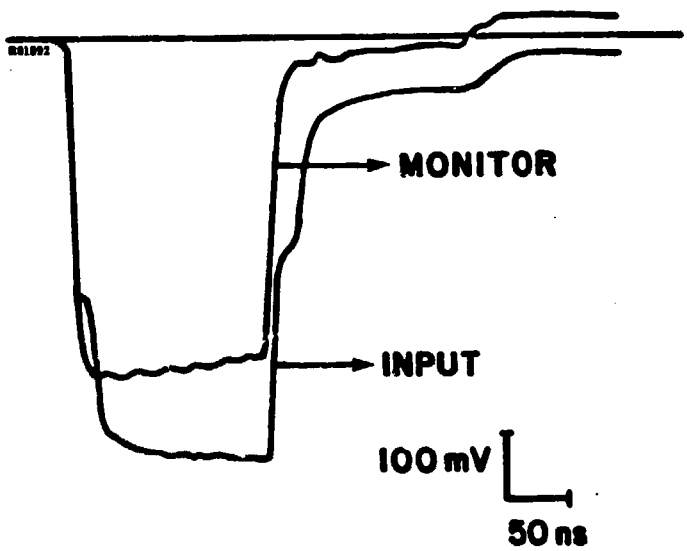

FIGURE 5. CALIBRATION CURVE FOR DIODE VOLTAGE MONITOR AT 100 mV/div AND INPUT VOLTAGE AT 750 V/div.

ORIGINAL PAGE IS
OF POOR QUALITY

3.1.2 Pulse Generator

Correct operation of the pulse generator was verified. This includes operation of the energy store, main switch, diode insulators, charging resistor, high voltage feedthrough and insulation from ground. Tests were performed up to 180 kV.

The energy storage, low inductance transmission lines showed no electrical signs of dielectric failure such as surface tracking or puncture. They will be visually examined further when the pressure tank is next opened.

The main switch was tested for approximately 500 cycles, 112 under high current arcs. There are no problems at this time.

The charging resistor was designed to prevent an overload of the power supply at 160 kV change. It functioned satisfactorily but needs to be replaced because the capacitance will be increased by 50%. The RC time constant for charging the energy store is now 0.8 second, and for continuous operation at 1 pulse every 3 seconds, an RC time constant of no more than 0.6 second is required.

The high voltage power supply cable is brought into the pressure vessel by a compression feedthrough that seals on the cable's outer insulation sleeve. This arrangement was acceptable electrically to 180 kV. However, the high pressure insulating gas was found to diffuse slowly down the braided inner conductor of the cable inside of the solid insulating layer. The gas escapes into the oil of the high voltage power supply, causing bubbles to form. Not bothersome now, the problem will be corrected in the next quarter by using a sealed feedthrough.

Pulse operation was tested by shorting out the diode through a plate with minimal inductance. Figure 6a shows the typical signal on the diode current monitor. This trace can be used to define the equivalent electrical parameters of the pulse generator, using the LRC circuit model shown in Figure 6b. The current follows an equation of the form:

$$I = I_0 \quad \exp -(R/2L)t \quad \sin (LC)^{1/2} t$$

where the exact solution to the circuit model was simplified, since $(L/R)^2 >> LC$. Here L is the total inductance of the pulse generator with the largest contribution from the switch and collector plate. The total capacitance C is that of the energy store pulse stray contributions. The total resistance R is believed to be mostly from the arc in the switch.

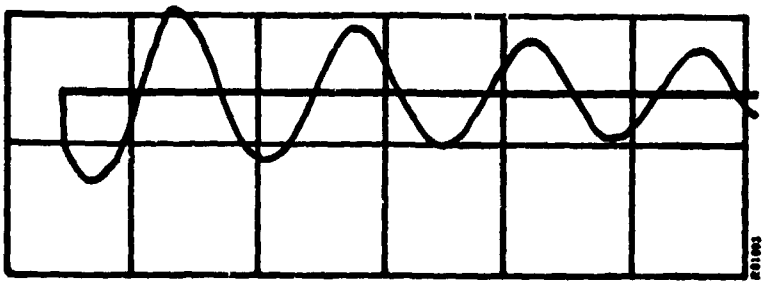

FIGURE 6a. CURRENT SIGNAL FROM PULSE GENERATOR WITH THE DIODE SHORTED OUT; 50 kV CHARGE, 34.5 kA/div, 50 ns/div.

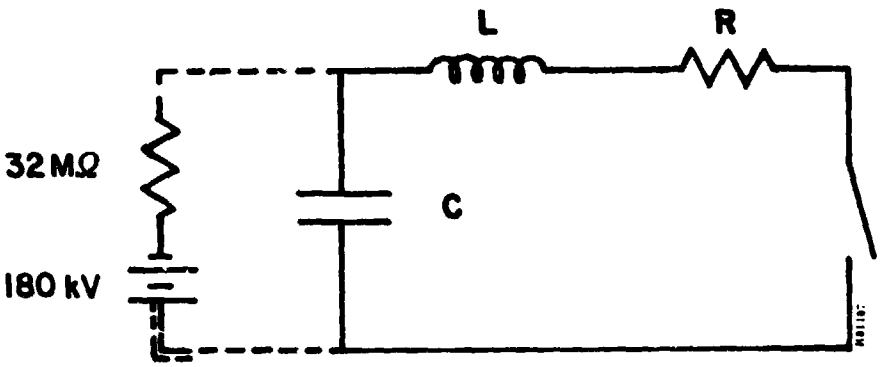

MEASURED	DESIGN
L 86 nH	100 nH
R .14 ohms	—
C 23 nF	24 nF

FIGURE 6b. EQUIVALENT CIRCUIT MODEL FOR PULSE GENERATOR WITH MEASURED PARAMETERS FROM (a)

The parameters R, L and C were determined from Figure 6a. The integral of the first half period of the curve was measured from a 5X blowup with a planimeter. This gave the total charge initially in the energy store (corrected for exponential decay) and the value of C = 23nF (±5%). The period of the oscillation is 280 ns (±5%), which is equal to $2\pi (LC)^{1/2}$, or L = 86 nF (±10%). The total resistance was determined from measurement of successive peaks on the curve, and R = 0.14 ohms ±10%.

A zeroth order approximation to the expected operation of the pulsed electron beam annealer can now be made. The desired fluence on the sample is approximately 1 J/cm^2 at an electron energy of 20 kV (off normal incidence). The required current is 40 kA in a 100 ns pulse. Measured values of L and C for the generator imply an effective impedance of approximately 4 ohms, compared to the 0.5 ohm impedance of this ideal diode. The ratio of diode voltage to charging voltage is approximately 1/9, or the required charging voltage for annealing is 180 kV. Energy efficiency is approximately 20%.

The actual impedance of the diode varies with time, and the pulse width will always be less than the half period (140 ns) of the generator. How close we can come to this model must be determined by experiment.

3.1.3 Diode Tests

The first setup used for diode tests was determined by the original design model. Diode parameters were then varied in a stepwise approach to the optimum electron beam required for annealing.

The variable parameters are cathode radius, cathode-anode gap sample-anode gap, and applied magnetic field. To maintain precision alignment, with an allowed tolerance of only ±0.0005 inch for the cathode-anode gap, sets of spacers were machined. These variations for the gaps are given in Table 1. Cathodes varied slightly in thickness, affecting the gap measurements. Also, different sample mountings changed the anode-to-sample distance. Planarity, however, was maintained. Cathodes of three different radii were tested: 4, 4.5 and 6 inches. The magnetic field is a continuous variable; however, for initial experiments a null field (no current in coil, residual field 60 gauss) and a high field of 2 kG were tested. A listing of all parametric variations is shown in Table 2. Note that the charging voltage was initially limited to 125 kV until silicon samples were prepared for evaluation.

TABLE 1. PRECISION SPACERS FOR MECHANICAL GAPS (INCHES)

CATHODE-ANODE GAP (Tolerance 0.0002 inch)		SAMPLE-ANODE GAP (Tolerance 0.001)
0.394	0.1965	0.082
0.0591	0.2362	0.121
0.0787	0.2756	0.157
0.1181	0.3150	0.280
0.1575		0.476

With 6-inch cathode, C-A gap was 1, 1.5, 2, 3, 4, . . . mm.

For sample distance, spacings were 2, 3, 4, 7, 12 mm

TABLE 2. PARAMETRIC MATRIX FOR DIODE TESTS

Exp't	Cathode Radius (in.)	Cathode-Anode Gap (in.)	Sample Anode Gap (in.)	Magnet Field (kG)	Charging Voltage (kV)
1	6	0.098 0.197	0.092 0.215	0 2.0	25, 50, 100, 125
2	4	0.116	0.188	0, 1.6	25, 50 100, 125
3	4	0.092, 0.110 0.135	no anode	0, 2.0	140
4	4	0.098	0.212 0.171	0, 0.18, 0.36, 0.72 1.0, 2.0	140, 150 160
5	4.5	0.108	0.171	0.7, 1.0	150, 160 170, 180

In any experiment, all combinations of given parameters were tested. Some variation in gaps were caused by different cathode thickness and sample mounting.

Diode current and voltage traces were digitized on equipment designed by Spire Corporation, written on magnetic tape and analyzed by a computer. The signal from the voltage monitor was corrected for inductive effects ($L_d dI/dt$), where L_d is the diode inductance, approximately 5 nH. A much smaller correction for the effective equivalent circuit model of the voltage monitor was also included. The code also calculates the perveance of the diode as a function of time, the electron energy spectrum, the total energy and the total charge for the pulse. A typical example is shown in Figure 7. The noise is due to the large dI/dt correction.

Correct functioning of the diode was verified by measurements of perveance. The perveance is defined as $I/V^{3/2}$, and is a geometrically determined quantity for planar, nonrelativistic, space-charge-limited electron beam diodes. For MKS units (amperes, volts, meters) its value is given[1] as:

$$I/V^{3/2} = 2.33 \times 10^{-6} \pi \ r^2/d^2$$

where I and V are the diode current and voltage, respectively; r is the cathode radius; and d is the cathode-anode gap. As shown in Figure 8, the perveance is a time-dependent function. This arises from the plasma which forms at the cathode at the start of the pulse and drifts to the anode at a constant velocity. In higher power diodes a plasma may also form at the anode and drift in the opposite direction.[1] Thus the value of the cathode-anode gap should be written as:

$$d = d_o - vt$$

where d_o is the initial gap, v is the closure velocity due to plasma drift and t is time. The value of v is approximately 2.5×10^4 m/s, and the theoretical curve is plotted in Figure 8 using this value. Agreement between the curves indicates that the diode is operating as expected.

In Figure 9, the value of $I_p/V_p^{3/2}$ is plotted as a function of r^2/d^2. Here I_p and V_p are the peak diode current and peak diode voltage (excluding the initial spike), respectively. Each point on this graph represents one of the 112 shots taken during the initial tests. The few points which lie off the line shown for $d=0.5\ d_o$ represent a diode configuration where the gap did not close before the end of the pulse. In other cases, the

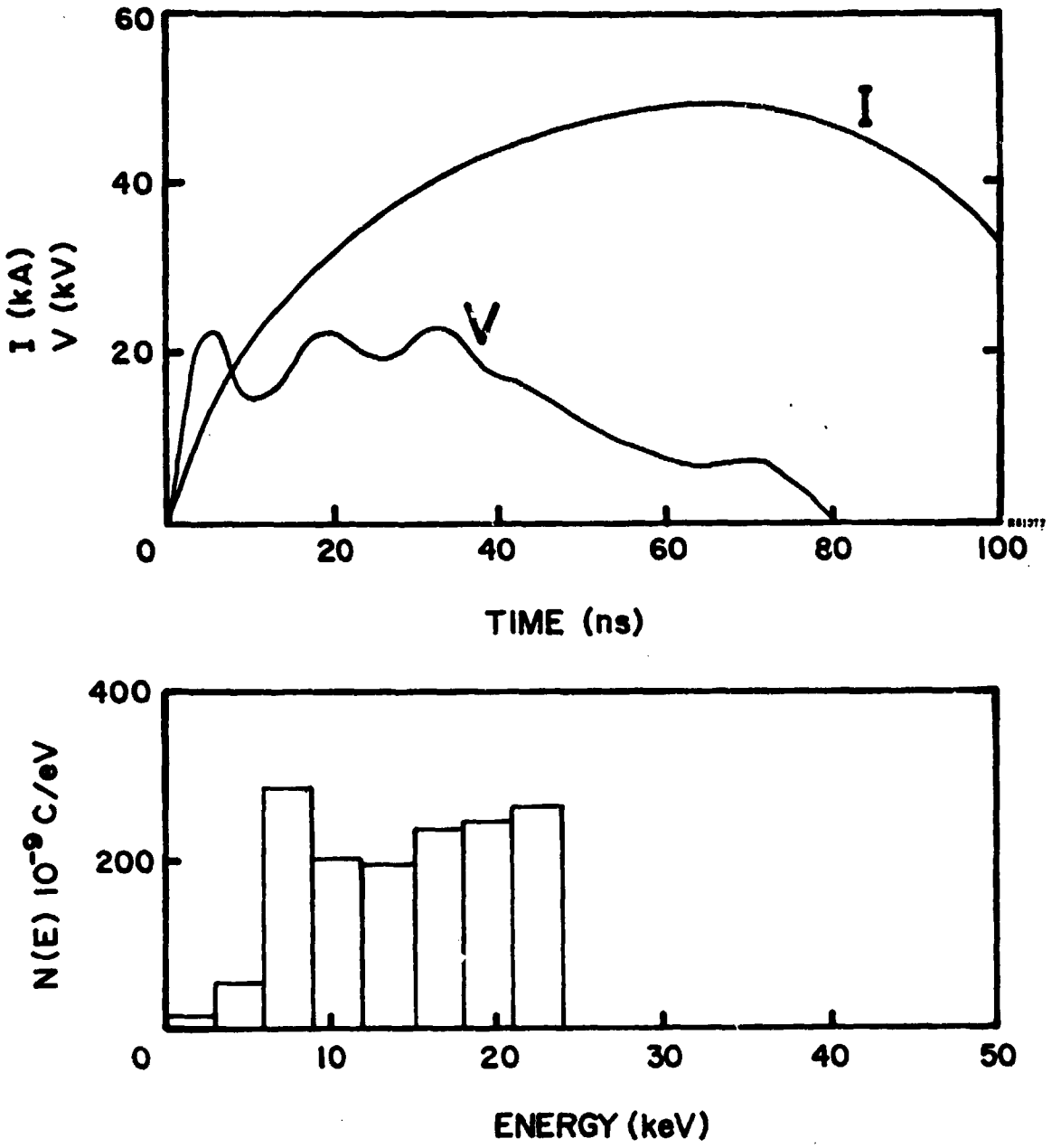

FIGURE 7. TYPICAL CORRECTED DIODE VOLTAGE, CURRENT AND ELECTRON ENERGY SPECTRA FROM COMPUTER CODE EBSPEC

ORIGINAL PAGE IS
OF POOR QUALITY

ORIGINAL PAGE IS
OF POOR QUALITY

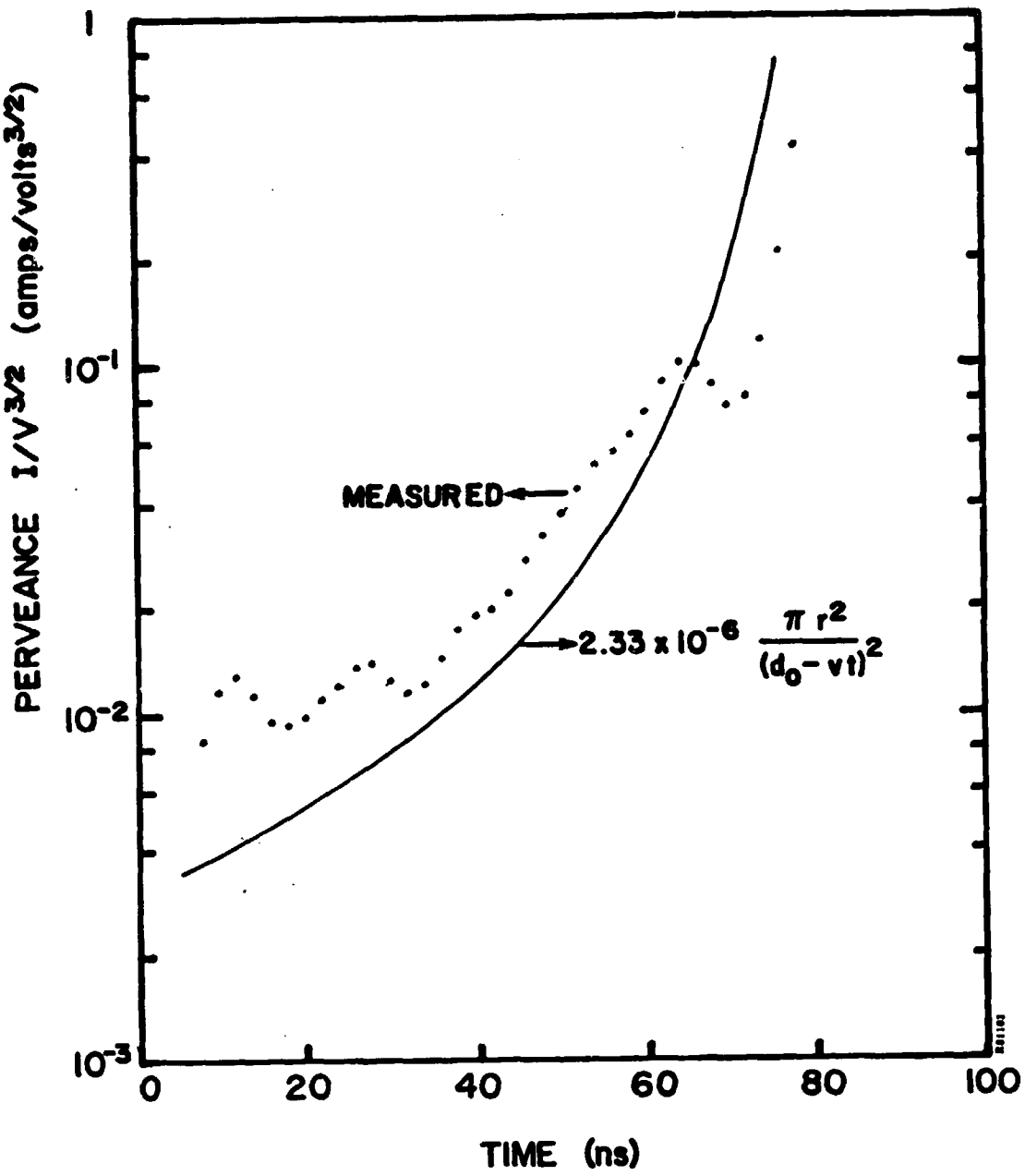

FIGURE 8. MEASURED AND MODELED DIODE PERVEANCE FOR PULSE SHOWN IN FIGURE 7.

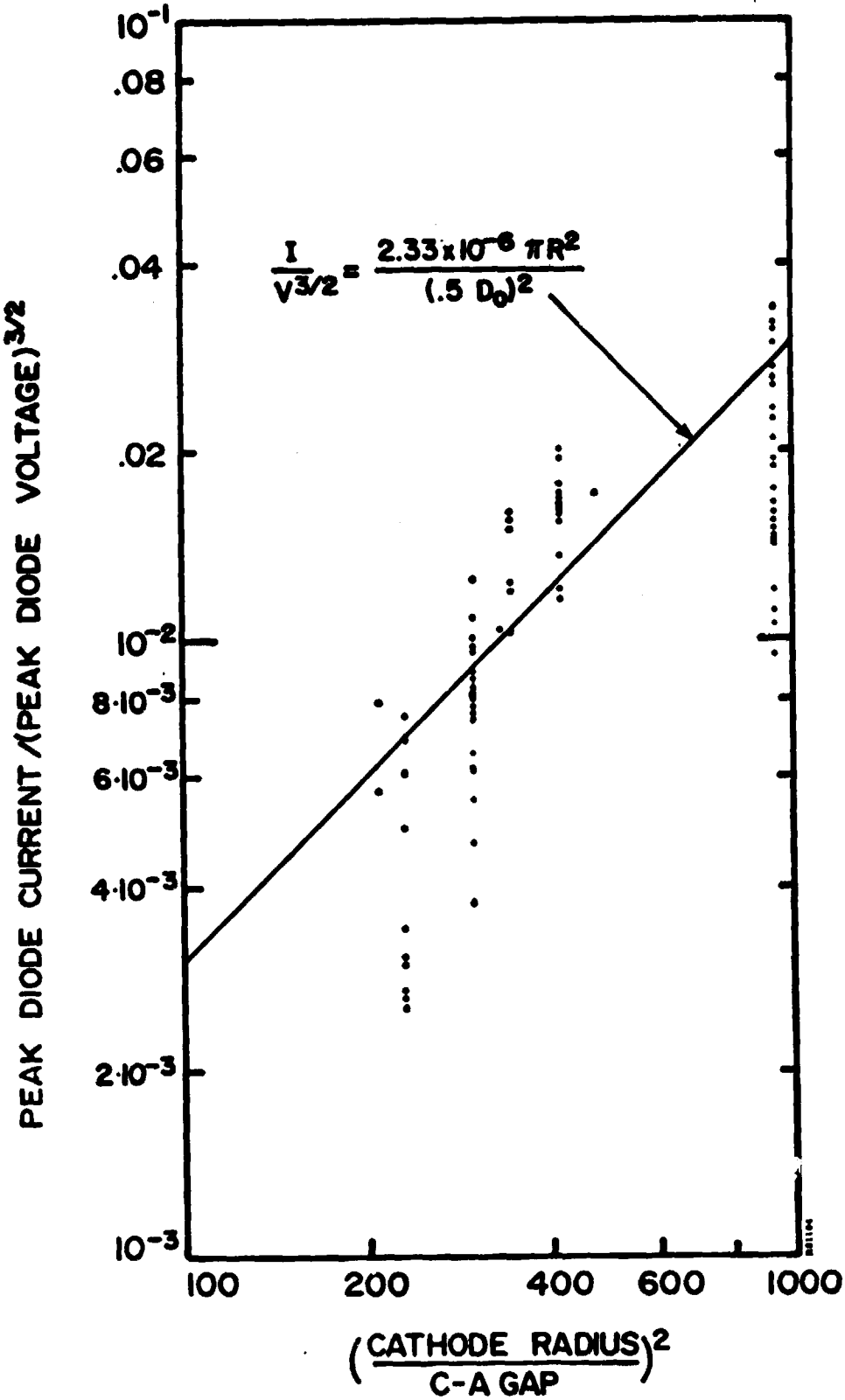

FIGURE 9. PERVEANCE AT MAXIMUM POWER VERSUS R^2/D^2 FOR SPI-PULSE 7000 INITIAL TESTS

drifting plasma did short out the diode (end of pulsed electron beam) before the pulse generator could reverse the current flow. Hence the average cathode-anode spacing was 0.5 d_o. Scatter in the data for large values of r^2/d^2 is caused by noise in the monitor signal, making interpretation difficult.

The behavior of the diode in all these experiments followed the theory and can be modeled easily.

3.1.4 Annealing Experiments

Initial annealing experiments were divided into two phases: (1) use of wafers as witness plates and (2) optimization of parameters for annealing.

The use of witness plates is required to verify electron beam uniformity on a small scale. The calorimeter samples the beam at 29 isolated points, with a minimal sampling area of 0.3 cm^2 at each point. Variations on the scale of 1 mm or less will not be seen by this diagnostic. Since the cathode and anode have patterns with 0.5 to 1.0 mm scale, the uniformity must be checked at this level. Ion-implanted wafers, when pulsed at fluence levels near the threshold for annealing, are ideal for this purpose.

Two lots of twenty-four 100 mm diameter wafers were prepared. All wafers were 14 mils thick, 1-2 ohm-cm boron doped, (100) silicon with lapped but not polished surfaces. The wafers were bright-etched and implanted on one side with 2.5×10^{15} ions/cm^2, 10 keV phosphorus. This is an optimum implant for a front junction of an n+pp+ solar cell, developed under a previous JPL contract.[2]

Initial samples were placed directly under the cathode, without an anode, to test the possibility of pulse processing in the simpler configuration. The electron beam showed a marked tendency to arc towards the wafer edge, even though the sample holder had an optimal configuration, with minimal surface distortion from a plane. This effect caused damage at the wafer edge. Over the remaining area of the wafer the average fluence (over about 1 cm^2) was excellent but had large variations on the millimeter scale of the cathode pattern. The geometry was changed to the cathode-anode-sample setup.

When the sample was placed behind the anode mesh, at a distance of 0.1 to 5.0 mm, two competing effects were visible. Very near the anode there was shadowing from the mesh wires; however, the pattern from the cathode was no longer discernible. Further from the anode, beyond 3 mm, the electron beam had a strong tendency to focus itself on the axis. The ratio of fluence on axis to that at a radius of 5 cm was about a factor of 3.

Adjusting the magnetic field greatly influenced the focusing action of the electron beam. At 2 kG the electron beam emission was confined to the outer edge of the cathode, and only a ring shaped hollow beam was recorded at the position of the sample. With appropriate charging voltage a uniform 7.5 cm diameter electron beam pattern was imaged using a magnetic field of 700 gauss. The pattern did not photograph well and cannot be included in this report. At about 1 kG the beam has a diameter of 10 cm but had sufficient energy for annealing only at a charging voltage of 180 kV. Approximately 80 percent of the area of the 100 mm wafer was annealed. The off-center pattern was traced to a mechanical misalignment of the lifter mechanism which is being corrected.

Annealing tests can only begin after determination of reasonable beam parameters. The sheet resistance of the sample varied from 27 to 43 ohms/sq in the annealed region. It is expected that a correction of the centering and magnetic field should yield improved results in the next quarter.

Modifications to the pulse generator to increase the number of energy storage liners and procurement of a higher voltage and current power supply are required. These changes will allow for improved service life at the required repetition rate for annealing 100 mm diameter wafers.

3.1.5 Material Development

A few material development tests were performed which are indirectly related to development of the optimal electron beam for annealing 100 mm wafers. These were cathode and anode tests.

The initial 6-inch diameter cathode for the SPI-PULSE^{TM} 7000 was made of copper impregnated graphite. This material has superior electrical and thermal properties to the very high purity, high density graphite used to date for this application. The material functioned well in limited early testing. Lifetime for over 10^6 pulses is sought, and that test must wait. With somewhat different electrical parameters, a test of 150,000 pulses of a similar space-charge-limited field emission diode was performed[3] without any degradation of the cathode, although the anode did wear slowly.

A test of anode wear was conducted at Spire. Currently, this diode component is made of fine tungsten woven wire and stretched tight for planarity. Repeated thermal cycling causes the wire to become brittle, and it eventually breaks under the tensile load. The wire was never observed to fail by apparent melting or material removal. Nickel wire mesh of the same weave was tried. It showed no signs of melting or other wear and no distortion or hardening after 700 pulses at appropriate fluence levels. Further lifetime tests are planned on the 7000.

SECTION 4
PLANS

During the next reporting period efforts will continue to complete the overall system assembly and test program as outlined in Figure 10. Under completely automated microprocessor control, the wafer transport and pulse annealing sequential operation will be tested. Annealed test wafers will be evaluated for optimization of the SPI-PULSE 7000 operating parameters.

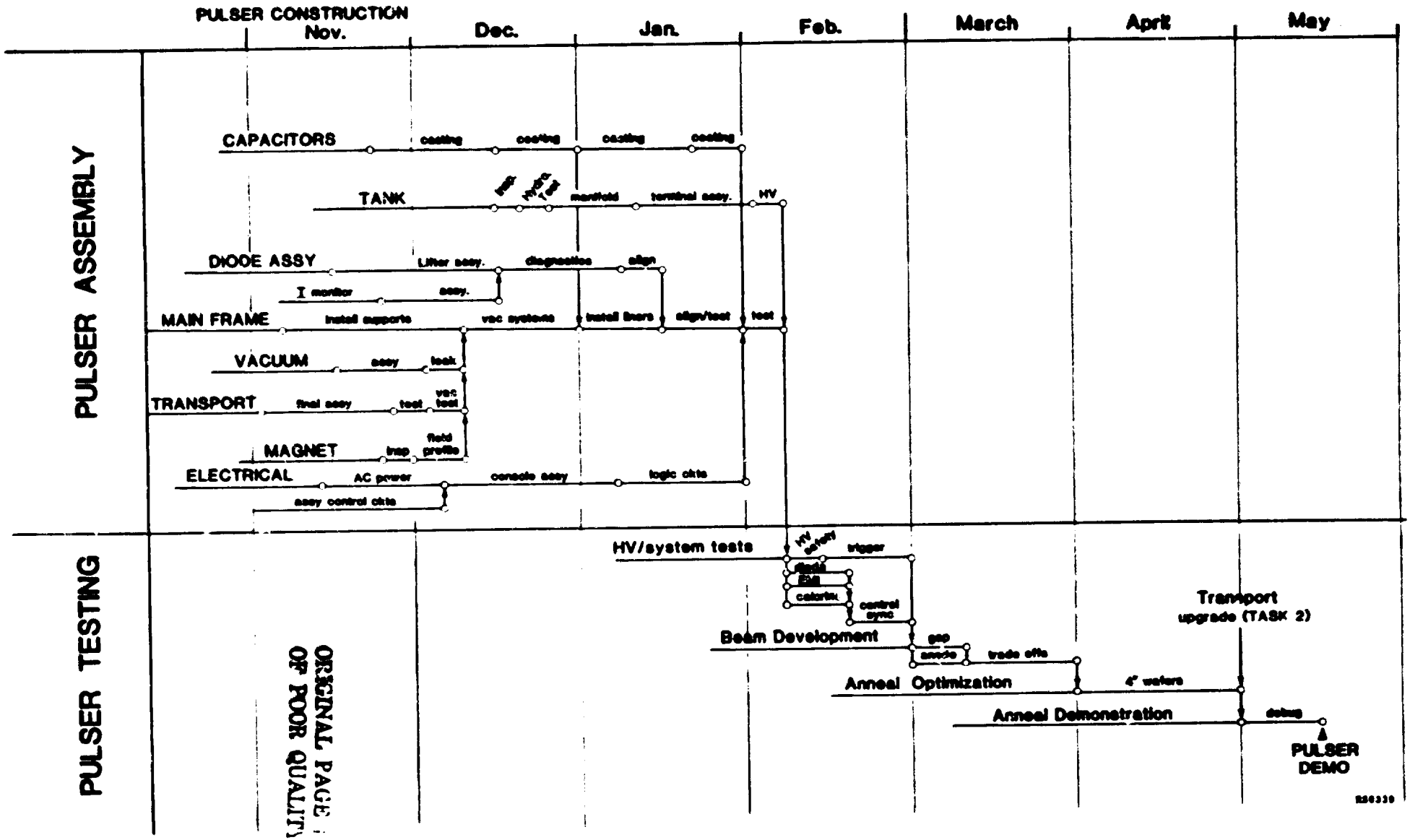

ORIGINAL PAGE IS OF POOR QUALITY

FIGURE 10. SPI-PULSE 7000 ASSEMBLY AND TEST SCHEDULE

SECTION 5
SCHEDULE

Figure 11 shows the projected schedule for Task 1, "Pulsed Electron Beam Subsystem Development".

PRECEDING PAGE BLANK NOT FILMED

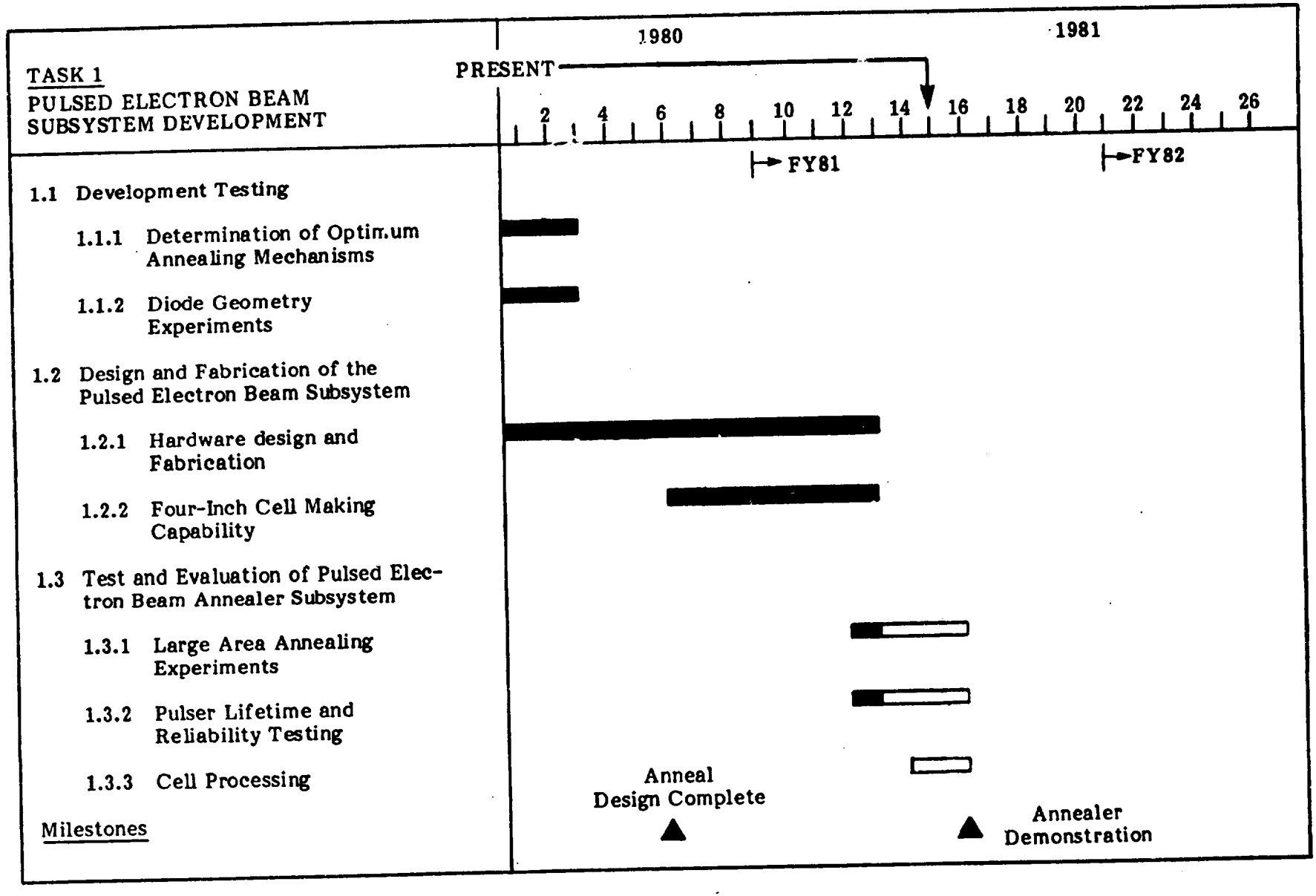

FIGURE 11. TASK 1 SCHEDULE

SECTION 6

PROGRESS ON TASK 2 - WAFER TRANSPORT SYSTEM DEVELOPMENT

6.1 TRANSPORT DESIGN AND FABRICATION

The new entrance "Y" track design and fabrication subcontracted to Brooks Associates is well underway and is scheduled for delivery to Spire in mid-May. In order to couple the 50 carrier cassette elevator entrance and exit locks with the "Y" tracks of the processing chamber, 20-inch-long, three-phase transition track sections have been designed. Delivery of these interconnecting manifolds is expected in early June.

For elevator control, a self-contained dedicated logic module has been selected. This module contains all the circuitry required to sequence the vacuum solenoid valves in response to input switch closures as given by a preset elevator end station sequence.

Since transport track speed must be held constant for accurate process timing, motor speed controls have been designed to phase-lock the track to an external frequency generated by the microcomputer. Chopper wheels used with optical interrupters will provide the speed feedback loop element.

SECTION 7
PLANS

It is anticipated that the vacuum system modifications and the additional hardware and software required to operate the double "Y" track transport system will be delivered and become operational during the next reporting period.

SECTION 8
SCHEDULE

Figure 12 shows the projected schedule for Task 2, "Wafer Transport System Development".

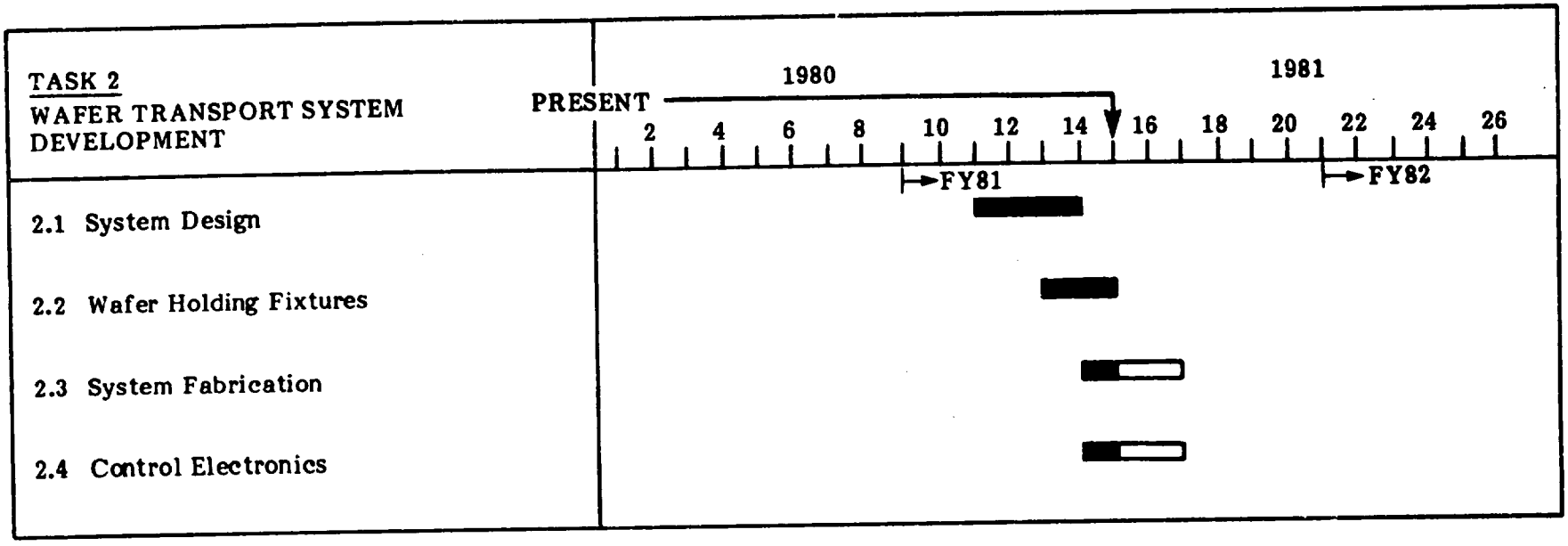

FIGURE 12. TASK 2 SCHEDULE

ORIGINAL PAGE IS
OF POOR QUALITY

REFERENCES

1. R. K. Parker, R. E. Anderson and C. V. Duncan, J. Appl. Phys. 45, 2463 (1974).
2. Spire Corporation, Final Report No. 10052, JPL Contract 954786.
3. M. T. Buttram, IEEE Trans. Nucl. Sci. NS-26, 4183 (1979).